Wear 328-329 (2015) 77–88

Contents lists available at ScienceDirect

Wear

journal homepage: www.elsevier.com/locate/wear

# *In situ* running-in wear assessment in multi-asperity nanotribology

Philippe Stempflé [a,*], Richard Kouitat Njiwa [b]

[a] Institut FEMTO-ST (UMR CNRS 6174 - Université de Franche Comté – CNRS – ENSMM – UTBM), 15B Avenue des Montboucons, F-25030 Besançon Cedex, France

[b] Institut Jean Lamour - MMNPS (UMR CNRS 7198 - INPL - Nancy University), Ecole des Mines, Parc de Saurupt, F-54042 Nancy Cedex, France

ARTICLE INFO

*Article history:*
Received 16 September 2014
Received in revised form
15 January 2015
Accepted 19 January 2015
Available online 27 January 2015

*Keywords:*
Running-in
Multi-asperity nanotribology
Nanowear
Tribolayers
Nanoindentation
Thin coatings

ABSTRACT

Wear analysis at the micro/nanoscale appears as a great challenge for MEMS/NEMS devices. At this scale classical *post mortem* analysis – like profilometry or AFM assessment – often failed because (i) the error in wear assessment owing to the elastic recovery is no longer negligible at this scale and (ii) the presence of nanometric *tribolayer* within the contact cannot be take into account when the contact is opened afterward. So, this paper deals with an *in situ* wear assessment based on a *triboscopic* approach where the final position $z_f$ of the ball is known without opening the contact because its vertical position is assessed at every instant of the process. This *triboscopic* assessment considers the initial approach of the surfaces $z_0$ and gives the wear rate by taking into account the presence of any *tribolayer* within the contact. It requires some corrections as (i) the tilt of the sample and (ii) the initial displacement of the surfaces, which is a function of the mechanical properties of the samples. The latter are determined by using an inverse method combining spherical nanoindentation and boundary element numerical simulations, which are both described too. Validation and application of this *in situ* approach to the running-in wear assessment of thin *soft* and *hard* coatings currently used in MEMS manufacturing are finally presented.



## 1. Introduction

At the micro/nanoscale wear analysis is a great challenge, especially for MEMS/NEMS devices that can be strongly affected by various surface phenomena, such as friction/stiction, micro- and nanoscopic wear, surface contamination and environmental effects [1–8]. Besides, nanowear mechanisms met in various microsystems are generally closer to the *polishing* process in terms of wear rate [9] than the classical mechanisms of *abrasion* [10], *adhesion* [7] or *ploughing* [4,11,12]. This peculiar wear process mainly results from the combination of a low contact pressure and a *closed* multi-asperity tribocontact that acts as a *triboreactor* at the micro/nanoscale [13–17], where thermal effects [18], chemical and physico-chemical interactions [19,1,20,21,7], environment's influence [14,22–24,15,19,25], and *tribolayer* are likely to control the tribological behavior, as a self-organization process [26,27,15,16,18,17].

Currently, topographical assessment is commonly used for analyzing wear at this scale [3,2,11,28,29]. Wear is then measured by determining the depth (or volume) of the wear track at the end of the test with a profilometer [10,30,21,23,31,15,16]. However, it is worth noting that this *post mortem* assessment is only suitable when the wear level is much more significant than the deformation one. Otherwise the error on the wear value due to the elastic recovery is no longer negligible [30,32,31]. In addition, this approach clearly assumes that only the *mechanical* component of wear occurs. This is generally true in a LFM/FFM experiment that simulates a *mono-asperity* contact with an AFM tip [10,21,33,34,17,35], but not any more in a real MEMS displaying many asperities [1,20,36,37,7,22,38,25,17]. In the latter case, *physico-chemical* aspects are superimposed on the *mechanical* ones. As a result, *adhesive* wear component also occurs leading to the formation of a self-organized *tribolayer* that usually controls both the friction and wear behaviors [39,27,26,15,16,18]. Thus, whatever its intrinsic accuracy [32,30], the main drawback of the topographical assessment is that any measurement is always carried out after the contact opening, meaning the loss of all the existing relationships between the frictional evolutions and the wear events. Hence, while this classical *post mortem* approach generally fails in the presence of such *tribolayer,* a real-time wear assessment would be likely to consider any *dynamic* influence of *tribolayers* on the tribological behavior [40,14,23,24,17].

Interesting ways to study a continuous running-in tribological system in real-time were recently proposed by Scherge et al. [41,9] and Dienweibel et al. [42]. The former describes an *in situ* wear assessment that is based on a radionuclide-technique, as a thin layer activation method [41] while the latter, rather proposes a real-time wear assessment using an on-line topographical approach [43]. All these approaches might work successfully in the case of

* Corresponding author.
*E-mail address:* philippe.stempfle@ens2m.fr (P. Stempflé).

http://dx.doi.org/10.1016/j.wear.2015.01.033
0043-1648/

MEMS because of their own accuracy and extremely high resolution (typically 0.1 nm/h).

As a simpler alternative, this paper describes an *in situ* approach which allows us to study wear mechanisms occurring on the micro/nanoscale level by considering a *multi-asperity* contact under low contact pressures (several hundreds MPa) and relatively high velocities (several mm/s) as met in MEMS [17]. This *triboscopic* approach considers the initial deformation of surfaces and gives the wear rate by taking into account the presence of any *tribolayer* within the contact. This *in situ triboscopic* approach will be detailed in Section 2 and validated on reference samples (pure silver and gold) in Section 4. The method will be finally apply to the case of thin *soft* and *hard* coatings currently met in MEMS manufacturing [44–46].

## 2. Theoretical background and practical approach

### 2.1. Triboscopic approach

Let us consider an experimental device [17] consisting of a *ball-on-disc* nanotribometer in a linear reciprocating mode (see Fig. 1 and details in Section 3.1), which simulates a typical MEMS tribocontact – as a *comb drive* for instance [1,20,5]. A $Si_3N_4$ ball (Ø 1.5 mm) is mounted on a stiff lever designed as a frictionless force transducer and loaded onto a flat sample with a precisely known force using a closed loop. The friction force is determined during the test by measuring the deflection of the elastic arm. A real-time depth measuring optical sensor is used for studying any vertical displacement of the ball along the friction track (Fig. 1).

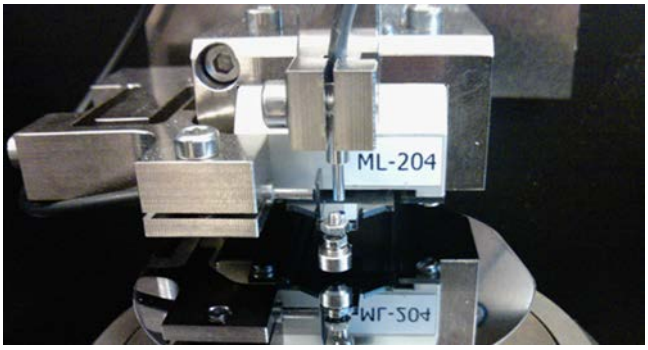


**Fig. 1.** Ball-on-disc nanotribometer and its real-time depth measuring optical sensor.

Results can be then compiled as a *triboscopic* approach giving simultaneously, and for each cycle:

- the *friction map* (Fig. 2a) plotting the evolution of the friction coefficient along the friction track;
- the so-called *depth map* (Fig. 2b) revealing any time-dependent wear process and/or potential build-up of a *tribolayer* within the contact [17]. However, this *depth map* cannot directly be assimilated to a real *wear map* because it includes: (i) the titling of the flat sample and (ii) a wrong value of the initial vertical displacement which actually corresponds to the initial elastic–plastic displacement of the flat sample under the initial applied normal load (so-called $z_0$).

Thus at the micro/nanoscales, and in contrast to the classical approaches of macroscale wear assessment, a preliminary accurate knowledge of the elastic–plastic behavior of samples is necessary because the deformation process strongly affects the precision of the *wear map* initialization. Keeping this consideration in mind, the nanotribological process – leading to the *depth map* (Fig. 2b) – can then be decomposed into four stages as follow:

- *Stage* 1: The *loading* that involves a vertical displacement $z_0$ from the initial surface. This value corresponds to the actual *zero-wear* vertical position. It can be computed by means of numerical simulation [47–49] – as a classical indentation problem of spherical punch on flat sample – as soon as the mechanical properties of each of the contact antagonists are known (*i.e.*, ball, coating and substrate in a general case).
- *Stage* 2: Starting from $z_0$, the *sliding* involves an evolution of the instantaneous vertical $z_i$ as a function of both the lateral displacement and the number of cycles. Thus, any variations of $z_i$ can reveal abrupt changes in the wear process. Note that $z_i$ normally increases when wear process occurs but it can also decrease – and even become lower than the initial displacement $z_0$ – in the presence of a *tribolayer* within the contact [17]. In practice $z_i$ can be extracted from data provided by the real-time depth measuring optical sensor from the *triboscopic* approach. However, since tribological tests are carried out in a linear reciprocating mode, a post-treatment of the raw depth data is needed in order: (i) to separate data from the *forward* and *backward* signals and (ii) to correct the sample tilt error. By considering the sign of the sliding velocity along the friction track, two *depth maps* (Fig. 3a and b) can be extracted from a *GNU Octave* script (http://www.octave.org/) and studied separately with the topographical software *Gwyddion* (http://gwyddion.net). Using the latter, sample tilt error along the friction

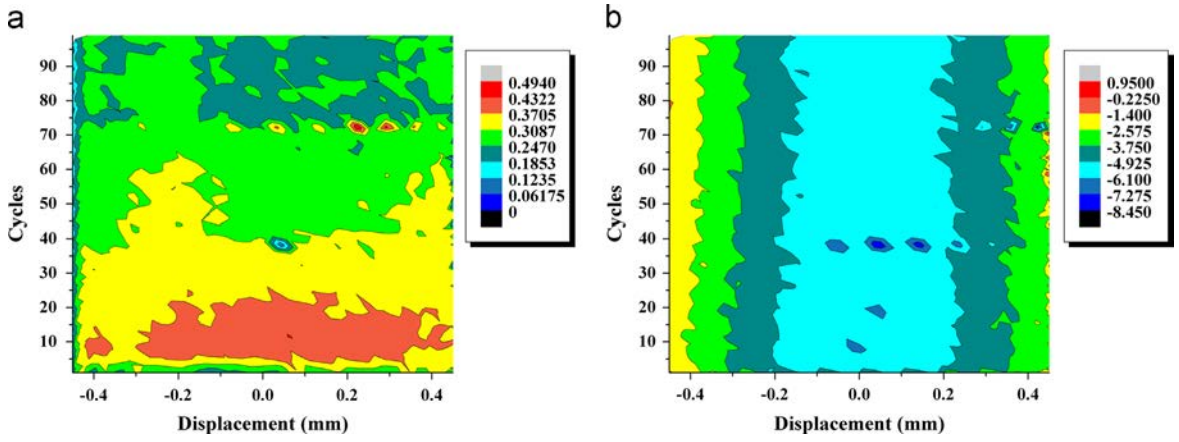


**Fig. 2.** Typical views resulting from a *triboscopic* approach giving simultaneously and for each cycle: (a) the evolution of the friction coefficient along the friction track (so-called *friction map*) and (b) the evolution of the ball depth within the friction track (the so-called *depth map* in μm). Samples: $Si_3N_4$/Silver – 45 mN – 100 cycles – 1 mm $s^{-1}$.

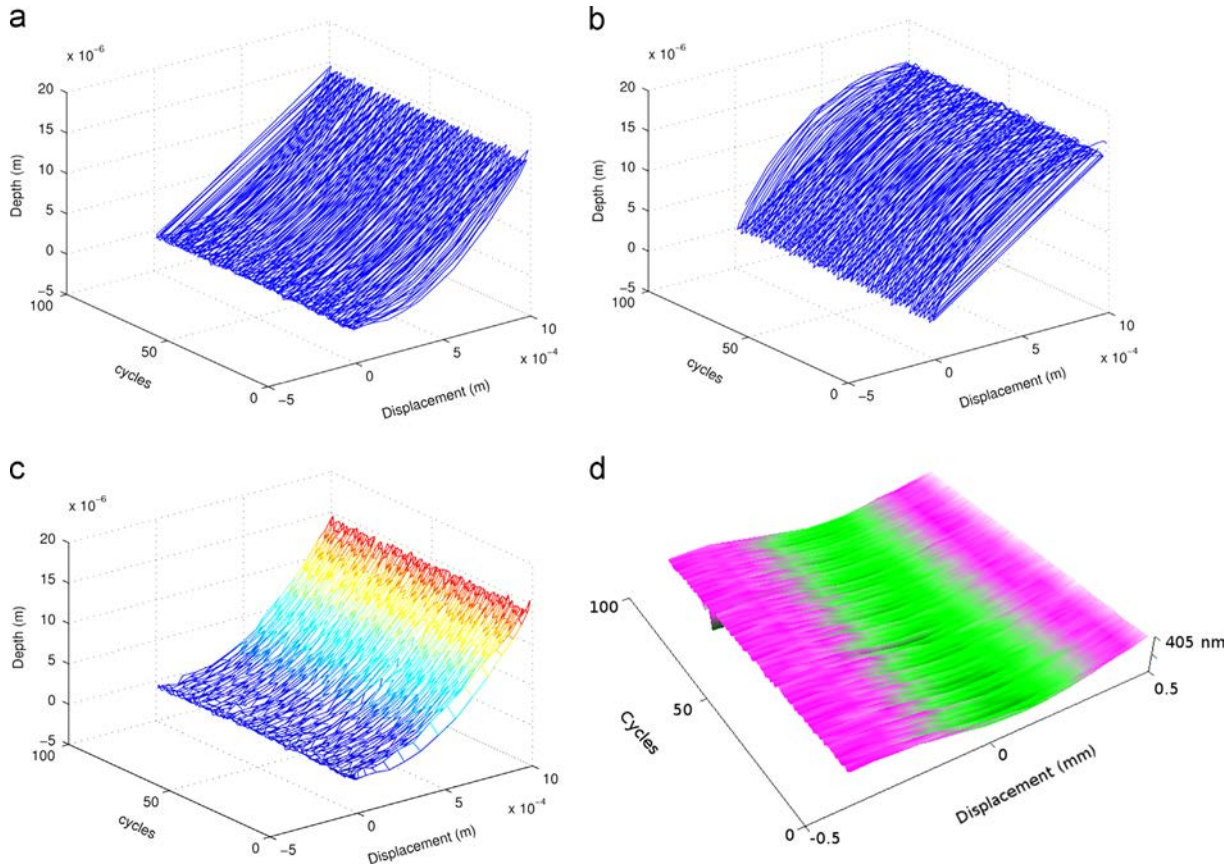


**Fig. 3.** Various stages of the *wear map* construction from the *depth map* raw data: extraction of the *forward* (a) and *backward* (b) *depth map*. Correction of the sample tilt error from the *forward depth map* (c) by applying a least mean square algorithm on each cycle (d). Samples $Si_3N_4$/Silver – 45 mN – 100 cycles – 1 mm $s^{-1}$.

track can be easily corrected on the *forward depth map* (Fig. 3c) by subtracting a least mean square slope on each cycle (Fig. 3d).

- *Stage* 3: At the end of *sliding* and just before *unloading*, the final displacement $z_f$ is assessed from the last cycle of the *forward depth map*. This value is strongly connected to various processes that are likely to occur during the tribological tests: reversible elastic and irreversible plastic deformations [50,8], stable and unstable fracture phenomena [51,52], wear processes [6,21,53,54,25], and materials phase transformations [27,53,55]. Thus, knowing the initial displacement $z_0$ and the final displacement $z_f$, an accurate estimation of the actual wear rate can be computed by $(z_0 - z_f)$. It is worth noting that the presence of any *tribolayer* is obviously detected by using this procedure.
- *Stage* 4: After *unloading*, the previous value $z_f$ can strongly decrease to a *residual depth* $z_r$ depending on the mechanical behavior of the samples after sliding. This residual depth $z_r$ corresponds to the one generally assessed by AFM profilometry [3,11,8]. Its value is generally controlled by the underlying friction-induced processes – like fracture [51] or sub-surface plastification mechanisms [50] – that are likely to occur during the test. Hence, $z_r$ is often very different than the real value of the wear depth corresponding to $(z_0 - z_f)$. The origins of this difference can be analyzed with the help of numerical simulations by studying how the mechanical properties of samples are modified by the tribological solicitations [52,56,35]. Note that the *in situ* method could be satisfactorily validated at this point by using a *post mortem* topographical approach with samples displaying a negligible elastic recovery in order to have approximatively $z_f \simeq z_r$. So, in that case, the *wear rate* could be computed by $(z_0 - z_r)$ instead of $(z_0 - z_f)$.

Fig. 3 summaries the construction of the *wear map* from the *raw* data that are extracted from the *forward depth map* given by the real-time depth measuring optical sensor. However, the initial vertical displacement ($z_0$) due to the applied normal load is not considered yet. This *zero-wear* position need to be computed, for each normal load, by means of numerical simulations implementing the indentation problem of spherical punch on flat coated sample, as shown in Fig. 4a. Considering this initial *offset*, the *actual wear map* (Fig. 4b) is then obtained by changing the initial depth value of the previous *forward wear map* (Fig. 3d) by the computed value of $z_0$ (Fig. 4a).

### 2.2. Assessment of the mechanical properties of the samples

As mentioned earlier, an accurate assessment of the elastic–plastic behavior of samples is needed because nanowear measurement is directly connected to an exact computation of $z_0$ that itself depends on the mechanical properties of the samples. Spherical nanoindentation appears as a suitable tool for determining these properties at the micro/nanoscales. However, classical approaches – *e.g.*, Oliver and Pharr or Field and Swain ones [57] – no longer work in the presence of thin coatings because they are too sensitive to the indentation size effect at low loads [57] and to the substrate effects at high loads [58]. Hence, an identification approach has been specifically developed in order to extract the intrinsic mechanical properties of thin coatings by avoiding the substrate's effects [59].

Basically our approach combines spherical nanoindentation ($R_i$ : 50 μm) with numerical simulations of the nanoindentation process. It never tries to experimentally assess the actual properties of the thin coating but always measures the combined properties of the compound (coating + substrate). Knowing these, and the mechanical properties of the substrate as well as the thickness of the coating, the mechanical properties of the thin coating are then identified by using a *hybrid* algorithm coupled with a numerical

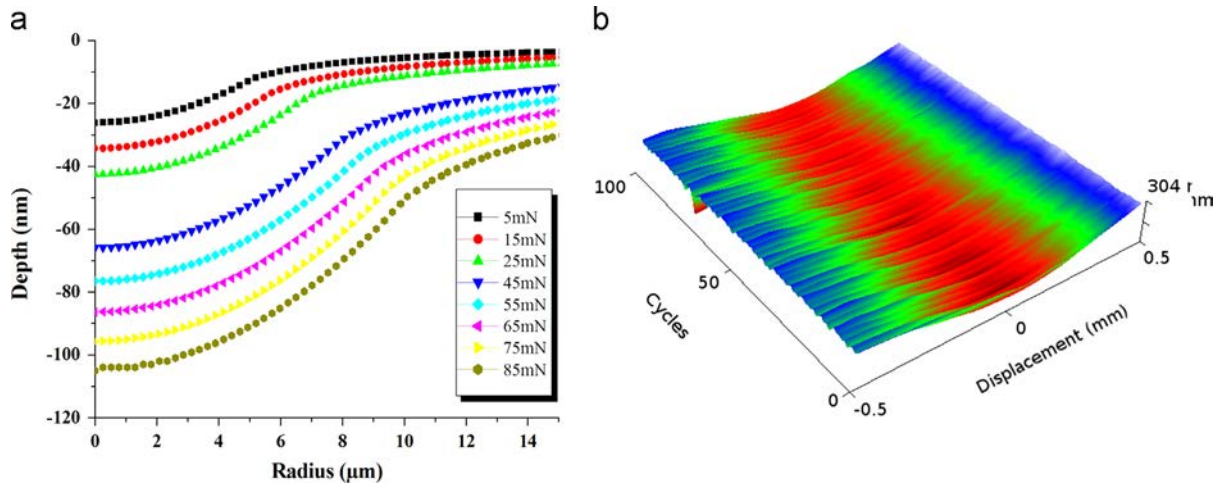


**Fig. 4.** (a) Determination of the initial vertical displacement $z_0$ for various normal loads using a boundary element analysis. (b) This value is integrated in the previous *wear map* (Fig. 3d) for initializing the first cycle. The correction is about 65 nm in this case. Sample $Si_3N_4$/Silver – 45 mN – 100 cycles – 1 mm $s^{-1}$.

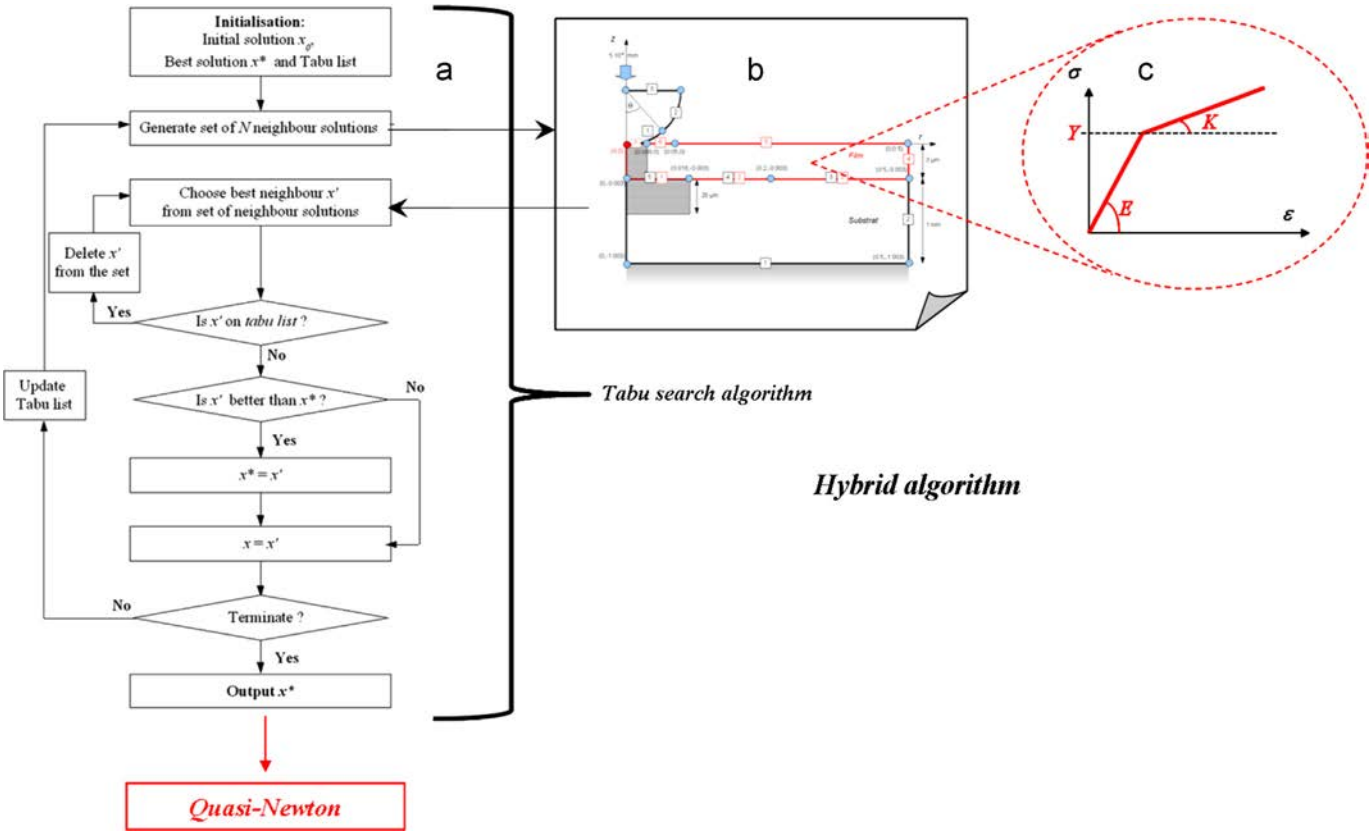


**Fig. 5.** (a) Hybrid algorithm driving a nanoindentation simulation code (b) for identifying the mechanical properties of a thin coatings (c).

code, which simulates the nanoindentation process [59], as shown in Fig. 5. This kind of algorithm is required owing to the complexity of the problem to be solved [60]. Indeed, as shown in Fig. 5, a *tabu search* algorithm [61] ensures the tracking of the global minimum by avoiding the local minima whereas a *quasi-Newton* one enhances the precision of the last optimum [60]. Details of this algorithm and its validations on various thin coatings and *tribolayers* are available in [59,16].

For a self-contained purpose, we just recall that its formulation consists of minimizing – by an iterative process – an *objective* function based on the difference between a vector of experimental data and the same data obtained with a numerical simulation of nanoindentation process. Four data, which are extracted from the load-depth curve of the compound (coating + substrate), are needed for the identification process [59]. An additional parameter is also required to take into account the amount of plastic deformation around the spherical indent [58]. The latter can be experimentally assessed from the topographical analysis of the residual imprint by using AFM profilometry. Thus, knowing the mechanical properties of the substrate and the thickness of the coating, our identification strategy – that is summarized in Fig. 6 – combines experimental and numerical steps as follows:

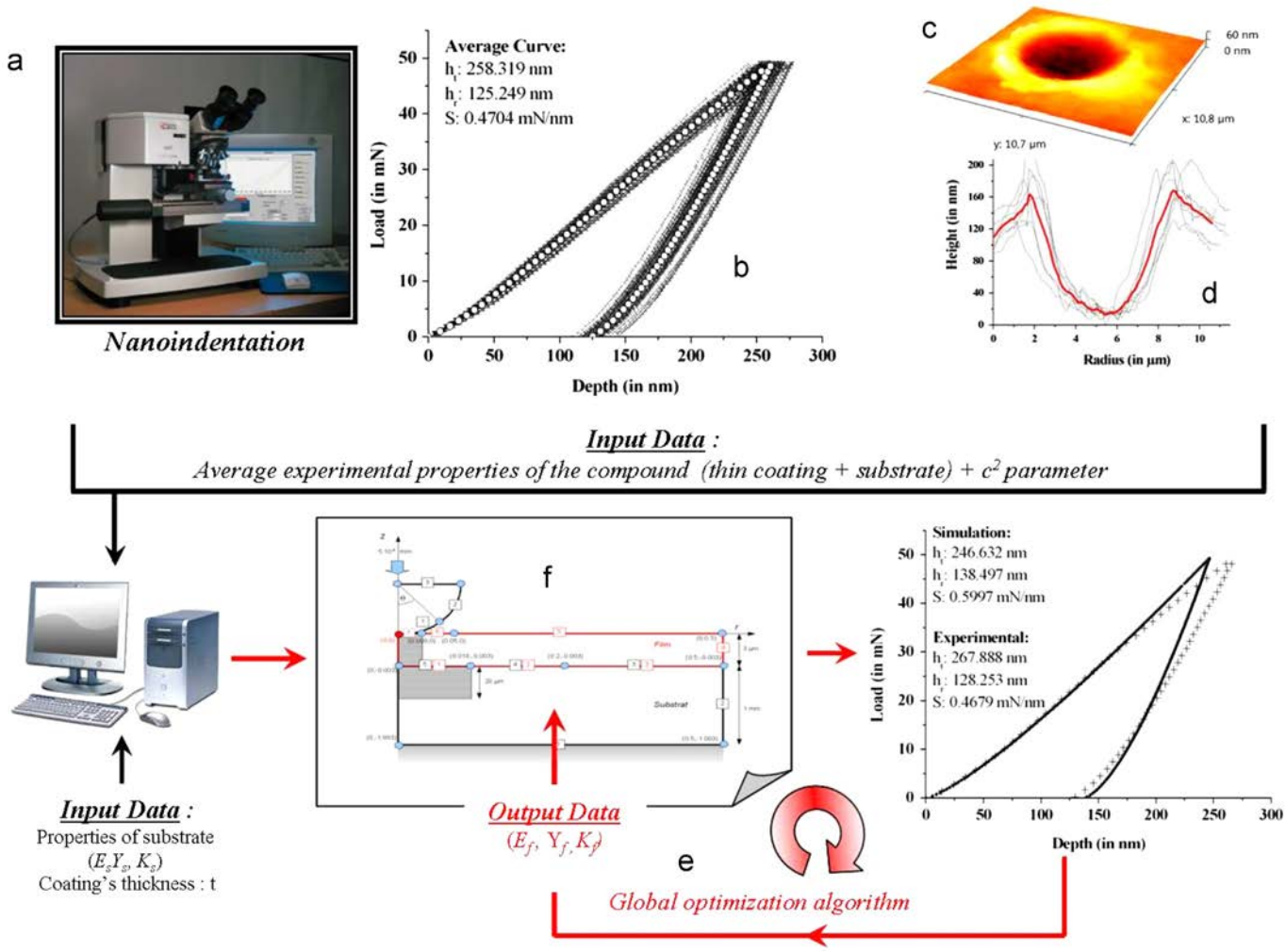


**Fig. 6.** Parametric identification procedure given the stress–strain law of thin coating knowing the mechanical behaviors of the compound (coating + substrate), the substrate and the thickness of the coating.

- Perform spherical nanoindentation test (about thirty for statistical validity) at relatively high normal load on the coated sample by using a 50 µm radius diamond indenter (Fig. 6a).
- Construct the average load–depth curve from the experimental indentation curves (Fig. 6b). Use this average curve, to determine: (i) the maximal depth $h_t$; (ii) the contact stiffness $S$ at the beginning of the unloading ; (iii) the residual depth $h_r$ and, (iv) a point of the loading curve: at 50% for instance.
- Make topographical assessment of the indent's imprint using AFM profilometry (Fig. 6c) and compute the experimental average $c^2$ parameter – proposed by Alcala et al. for characterizing the amount of *piling-up* or *sinking-in* around the spherical indent as a fraction of the maximum penetration of the indenter $h_s$ [58] – from the topographic profiles (Fig. 6d). The Alcala's procedure is used to:
  (i) establish the location of the contact radius, $a$, upon complete unloading;
  (ii) measure the value of $h$, the location of the contact area;
  (iii) calculate the difference $h_s - h = u_z$ at $r = a$ where $h_s$ is the maximum depth of penetration underneath the original surface;
  (iv) compute the quantity $1 - u_z/h_s$ which gives the value of $c^2$ (resolution better than 2%);
- Combine all these experimental values as a vector of experimental data and use them – in relation with both the substrate's mechanical properties and the coating's thickness – as *input* data of the *hybrid* algorithm (Fig. 6e and described in Fig. 5a), which drives the numerical code modeling the nanoindentation process (Fig. 6f) in order to identify the average mechanical properties of the thin coating.

As soon as the algorithm stopping criteria are reached [59], the identification process is stopped and the parameters of the stress–strain law of the thin coating are found and analyzed as shown in Fig. 5c. These latter are finally used for computing the initial vertical displacement $z_0$ in order to initialize the first cycle of the *wear map* (see Fig. 4a). The above algorithm is coded on *SCILAB* (http://scilabsoft.inria.fr) because it integrates some *Scilab functions* which avoid the development of classical routines [62].

### 2.3. Multiscale numerical simulations

Numerical simulations required for the wear assessment (Section 2.1) and for the nanoindentation testing (Section 2.2) are both connected to the same mechanical problem: the indentation of a flat coated sample with known film thickness by a spherical punch. The only differences between the two simulations are the radius and the material of the ball – *i.e.*, 50 µm radius diamond ball for nanoindentation tests, and 750 µm radius $Si_3N_4$ ball for nanotribological tests. Hence, the same numerical tool can be used in both cases. In this work, the boundary element method [52,51,63,49] is adopted for the solution of the indentation problems. In this context,

it is a well-established alternative to the powerful finite element method (see *e.g.* [56]) because of its ease to handle non-conforming contact problems with localized plastic zone [64,48].

For each model, the lateral dimension of the specimen is then adapted such that the results are undisturbed by end effects (Fig. 5b). As shown in Fig. 5c, the film and the substrate are both modeled as an elastic–plastic medium with a bi-linear stress–strain law – *i.e.* with three parameters: (i) the Young modulus $E$, (ii) the yield stress $Y$, and (iii) the strain hardening factor $K$ – enabling to model both *soft* and *hard* coatings [63,49]. Since the load applied on the punch is small enough – several tens of mN – the problem can be treated within the framework of the small perturbation hypothesis of the classical continuum mechanics [64]. The plastic problem is treated by the radial return algorithm, which is an implicit strategy based on the concept of consistent tangent operator insuring a good convergence during the identification process [49]. The classical approach requiring volume cells limited to part of the medium where plastic flow is expected is implemented as mentioned in [64] and shown in Fig. 5b. Our homemade code is programmed in *FORTRAN* for computing time efficiency [65,64]. Details of its implementation and validation on various indentation problems are available in [63].

## 3. Experimental part

### 3.1. Multi-asperity nanotribometer

The experimental device (Fig. 1) consists of a ball-on-disc *nanotribometer* manufactured by *CSM Instruments (Switzerland)* [17]. The friction force is determined during the test by measuring the deflection of the elastic arm ($K_x = 265.1$ N m$^{-1}$; $K_z = 152.2$ N m$^{-1}$). The 750 µm radius $Si_3N_4$ ball is loaded onto a flat sample with a precisely known force using the closed loop. The normal load and friction force resolutions are about 1 µN. Tribological tests are carried out in a linear reciprocating mode at room temperature (22 °C) under controlled environment (RH 35%). The normal load varies between 10 and 90 mN which corresponds to a contact pressure varying in the range 0.32–0.85 GPa. The stroke frequency, the stroke length and the stroke length resolution are 10 Hz, ± 0.5 mm, and 250 nm, respectively. The velocity and the sliding distance are 1 mm s$^{-1}$ and 0.2 m corresponding to 100 cycles.

A real-time depth measuring optical sensor has been specifically designed in order to study the time-dependent wear properties. The depth range varies from 20 nm to 100 µm with a resolution of about 20 nm. Results can be compiled as *triboscopic* views displaying both the *friction map* (Fig. 2a) and the *wear map* (Fig. 4b).

### 3.2. Nanoindentation

Mechanical properties of samples are assessed with a *Nano-Hardness-Tester* (Fig. 6a) provided by *CSM Instruments* (*Switzerland*) [15,49]. It is composed of two elements: an instrumented nanoindenter and a display system combining an AFM head (*SIScan Pro-ULTRAObjective*) and an optical microscope (enlargements × 50 and × 1000). These elements are linked with an electromechanical positioning system (X,Y), which allows a relocation of the sample between the indenter and the microscope with a precision of 0.5 µm. The vertical displacement and loading resolutions are respectively 0.03 nm and 1 µN. The compliance of the apparatus is 0.25 nm mN$^{-1}$. The indenter is a 50 µm radius spherical diamond indenter ($E_i$ : 1141 GPa, $\nu_i$ : 0.07).

The combined optical/AFM system gives the possibility to locate the indented zone with the optical microscope and to scan this zone after indentation in high resolution with the AFM contact mode. As mentioned earlier, AFM topography of the imprint is needed to compute the experimental $c^2$ parameter (Fig. 6c). The spatial resolution of the AFM is lower than 1 nm. The stiffness of the cantilever is 0.36 Nm$^{-1}$.

### 3.3. Post-mortem wear assessment

The *triboscopic* wear assessment provides an *in situ* wear rate leading to a final wear amount that needs to be *quantitatively* validated. *Post mortem* approaches might work for this purpose if the sample's contacting surfaces display a negligible elastic recovery as pure silver and gold, for instance [12]. Two complementary *post mortem* methods have then been chosen:

- (i) a topographical approach is used by means of a phase-shifting interferometric profilometer *ATOS MICROMAP* 570 ($\lambda$=520 nm) with a spatial and vertical resolution of 0.5 µm and 0.02 nm, respectively [17]. Worn volume is classically computed by integration of the height distribution, as detailed in [16];
- (ii) an accurate mass lost approach that uses a quartz crystal microbalance (QCM) provided by *Testbourne Ltd* (England). QCM is classically employed as an *in situ* approach (see *e.g.* [66]). However, it cannot be used like that in our case because the contact between the ball and the sample would influence the resonance frequency during the test. So, *post mortem* wear of 250 nm thick gold electrodes – deposited on AT-cut quartz crystal (Ø1 in and 330 µm thick) and submitted to nanotribological tests – has been evaluated by measuring the frequency *before* and *after* tribological tests. Knowing this frequency shift, the mass lost can be estimated using Sauerbrey's equation [66] as follows:

$$\Delta f = -N\frac{2f_0^2}{\sqrt{\rho\mu}}\frac{\Delta m}{A}$$

where $\Delta f$ (Hz) is the variation in frequency induced by the variation in mass $\Delta m$ (g), $\rho$ and $\mu$ are the crystal density (2.648 g cm$^{-3}$) and the shear modulus ($2.947 \times 10^{11}$ g cm$^{-1}$ s$^{-2}$) of quartz crystal, respectively. $A$ (cm$^2$) is the sensitive area corresponding to the electrode area (0.32 cm$^2$). $N$ is the overtone number, and, $f_0$(Hz) is the fundamental resonance frequency of AT-cut quartz crystal (5 MHz).

Sauerbrey's equation is well adequate here because the gold coating is thin and continuous along the quartz resonator [66]. So, QCM appears as a very accurate method for the *post mortem* wear assessment (precision around $10^{-9}$ ng cm$^{-2}$) because of its very high sensitivity constant ( ≈ 17.7 ng cm$^{-2}$ Hz$^{-1}$ for an usual 5 MHz quartz resonator).

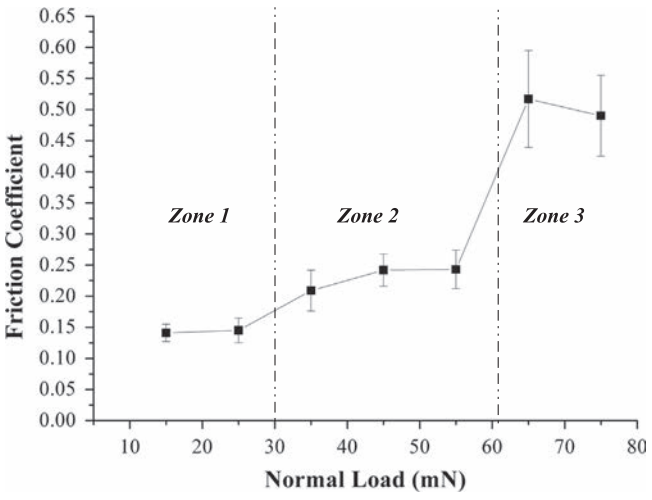


**Fig. 7.** Evolution of the friction coefficient vs. normal load ($Si_3N_4$/Silver, 100 cycles, 1 mm s$^{-1}$).

## 4. Results and discussion

### 4.1. Validation of the in situ triboscopic approach on reference samples

#### 4.1.1. Qualitative wear assessment

Fig. 7 plots the evolution of the friction coefficient with respect to the normal load obtained when a $Si_3N_4$ ball (Ø 1.5 mm) is rubbing on a pure silver flat sample during 100 cycles. Obviously, the friction coefficient increases with the normal load but two thresholds delimiting a *low* (*Zone* 1) and a *high* regime (*Zone* 3) can be noticed around 30 and 60 mN, respectively. Besides, a seizure phenomenon probably occurs in the *high* regime zone as suggested by the increase of the error bars. To understand what is really happening in each zone, results of the *in situ triboscopic* approach are plotted in Fig. 8.

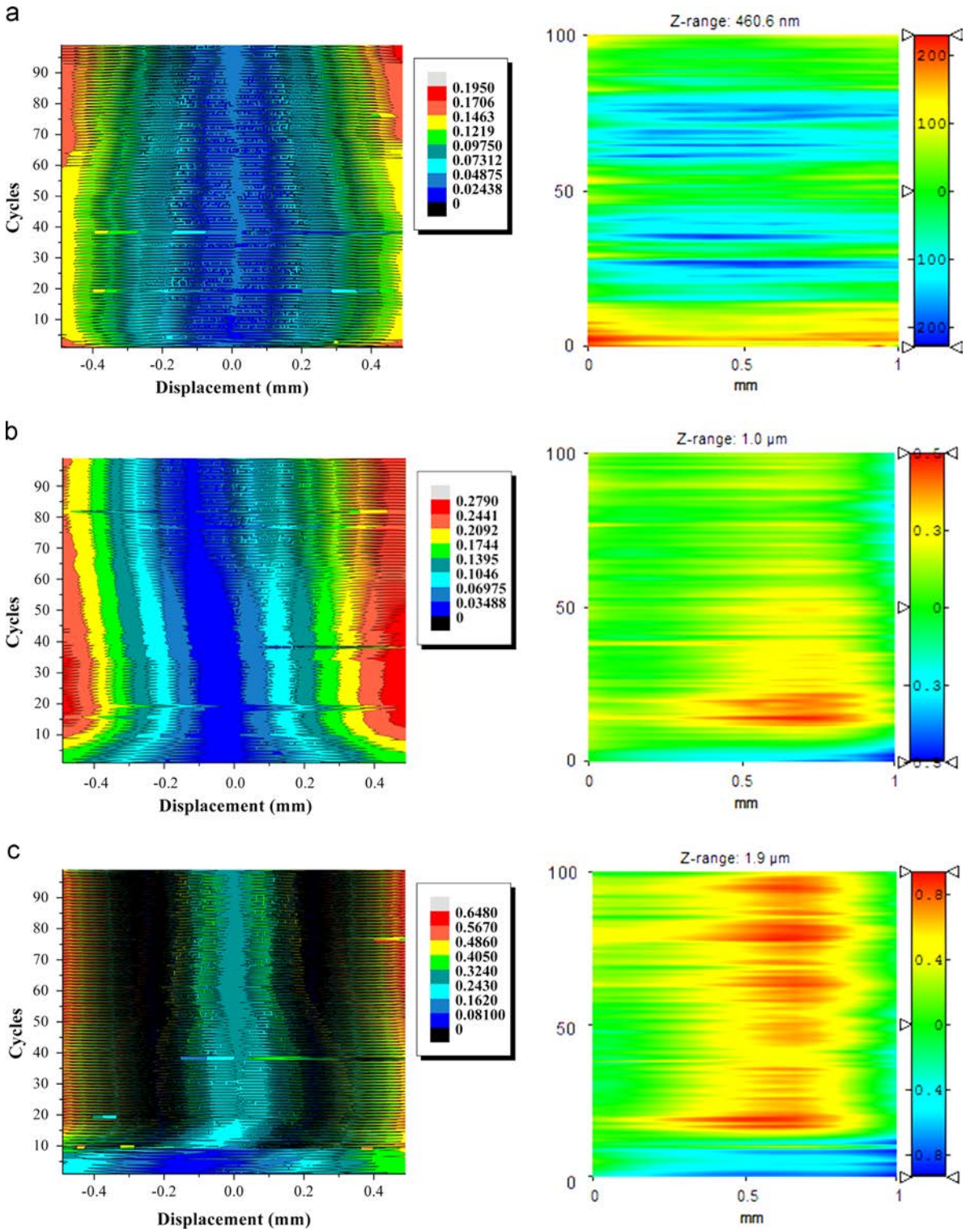


**Fig. 8.** *In situ* wear assessment of $Si_3N_4$/Silver for various applied normal loads (100 cycles, 1 mm $s^{-1}$). (a) Triboscopic view of the test carried out at 25 mN (*Zone* 1):*friction map* (left) ; *wear map* (right). (b) Triboscopic view of the test carried out at 45 mN (*Zone* 2): *friction map* (left) ; *wear map* (right). (c) Triboscopic view of the test carried out at 65 mN (*Zone* 3): *friction map* (left); *wear map* (right).

In *Zone* 1 (Fig. 8a), *friction* and *wear maps* are both quite homogeneous along the friction track and over time. Wear depth is rather low and never exceeds 461 nm at the maximum. However, when the normal load increases to reach the *Zone* 3 (Fig. 8b and c), *wear maps* reveal the presence of an adhesive *tribolayer* within the contact. Its thickness – and probably its *cohesion*, which is connected to its mechanical properties – increases with the applied normal load. Indeed, at 45 mN, the *wear map* reveals that the *tribolayer* is not sufficiently cohesive to stay in the contact (Fig. 8b); it is quickly destructed over time. In contrast, at 65 mN, (Fig. 8c), its *cohesion* – and hence, its mechanical properties – becomes strong enough for controlling the frictional behavior: a seizure phenomenon is then observed in the *Zone* 3 as soon as a *tribolayer* appears (around 10 cycles in the *wear map*). Thus, our *triboscopic* approach is sufficiently accurate for detecting any modifications of the *tribolayer* properties (cohesion and adhesive interactions).

As a result, *in situ wear maps* clearly provide *qualitative* information about the evolution of the mechanical properties of *tribolayers* within the contact. This information is crucial for analyzing the possible link between friction and wear process. Is it possible to get a *quantitative* wear rate assessment from this approach?

#### 4.1.2. Quantitative wear assessment

Two *post mortem* approaches are used for validating the *quantitative* wear prediction ability of our *in situ* method. Tribological tests (Ball $Si_3N_4$Ø 1.5 mm – 15 mN – 100 cycles – 1 mm/min) have been carried out on a quartz crystal microbalance resonator constituted by a piezoelectric 330 µm thick quartz substrate covered by two thin gold electrodes on each face (250 nm thick). For the sake of statistical validity, 20 similar tribological tests have been spread out on the resonator, as shown in Fig. 9a. In fact, there are at least three good reasons to use quartz crystal resonators here, as tribological samples:

- First, topographical assessment of the friction track at the end of the test makes sense because the stress–strain behavior of pure gold is known to be elastic-perfectly plastic [12]. Thus, $z_f \approx z_r$, as shown by the scar depicted in Fig. 9b.
- Second, since the hardness of the gold layer is quite low in regard to that of the quartz, only the gold layer should suffer wear during the tribological tests whereas the quartz substrate should display elastic deformation only. This assumption is clearly confirmed in the inset of Fig. 10, where the wear depth never overshoots the height of the gold layer. So, the *post mortem* QCM approach is also thoroughly licit for assessing wear rate of the gold electrodes.
- Third, since only the coating suffers wear, the elastic deformation of the substrate can be then easily computed, as shown in Fig. 4a, in order to determine the initial *offset* which initializes the *triboscopic* approach. Hence, the latter should also provide an accurate assessment of the gold layer wear process.

Keeping these considerations in mind, results provided by these approaches can be compared together:

(i) by using a QCM: the weight lost *after* 20 tribological tests has been computed with the Sauerbrey's relationship [66] from the frequency variations ($\Delta f = 25 \pm 7$ Hz). Thus, the average weight lost per test is about $118 \pm 15$ ng;

(ii) by using an interferometric profilometer: the worn volume has been computed for each track by integrating the distribution in height (Fig. 10) [16]. Average volume and surface of the tracks have been estimated for 20 tests at $5.53 \times 10^3$ µm$^3$ and $5.44 \times 10^{-2}$ mm$^2$, respectively. Knowing the worn material density ($\rho = 19.25$), the average weight lost per test is about $106 \pm 6$ ng.

(iii) using the *in situ triboscopic* approach: the assessment is carried out on various *wear profiles* extracted from each *wear map*, as shown in Fig. 11a. Typical *wear map* reveals that there is no any cohesive *tribofilm* within the contact but a continuous wear process. Debris are not agglomerated but clearly ejected outside the contact. As shown in Fig. 11b, the wear profile looks like the one we used to observe with an AFM tip (*i.e.*, for a mono-asperity contact). This is not really surprising if we consider the ratio between the hardnesses of gold coating and ceramic ball. Indeed, due to the contact pressure, the initial *multi-asperity* contact quickly becomes a *mono-asperity* one as soon as the first plastic deformation occurs in the gold coating. In addition, the wear amount is not a linear function of time. It rather follows a polynomial function ($R$=0.989) meaning that the wear rate strongly increases after the 70th cycle. Note that the wear rate also seems to be a function of the slider's position. So, the *wear map* appears

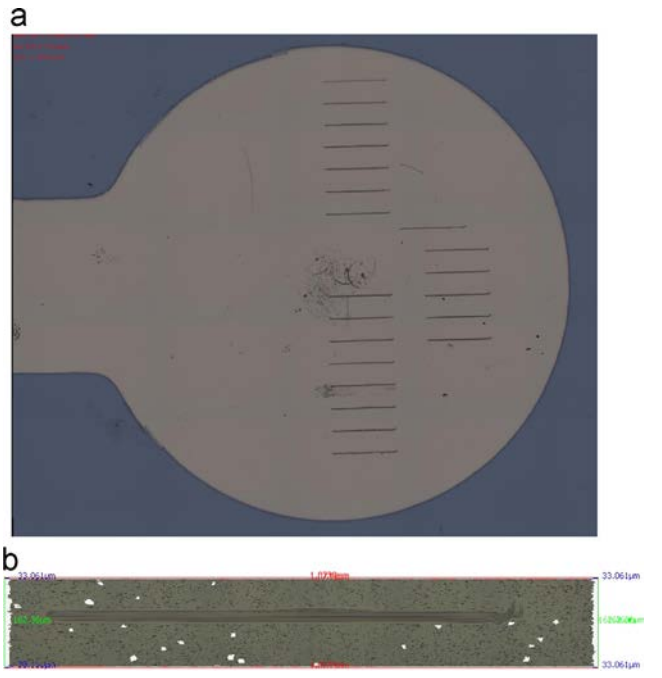


**Fig. 9.** (a) Nanotribological tests carried out on a quartz crystal resonator covered by gold electrodes. The mass lost per test is around 118 ± 15 ng ; (b) profilometric analysis confirming that only the gold layer is worn.

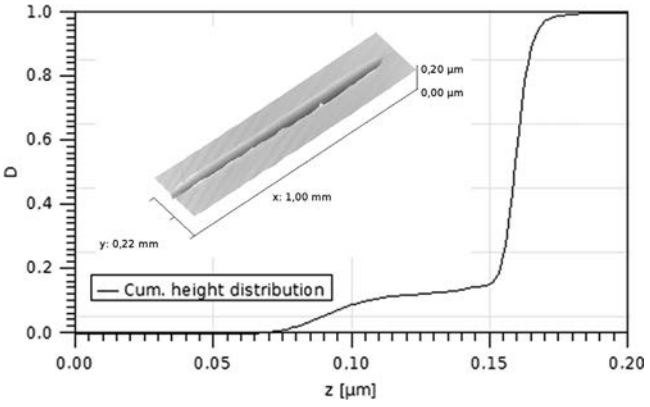


**Fig. 10.** Wear scar topographical analysis of a quartz resonator. The worn volume is computed by integration of the height distribution. The weight lost per test is evaluated at 106 ± 6 ng.

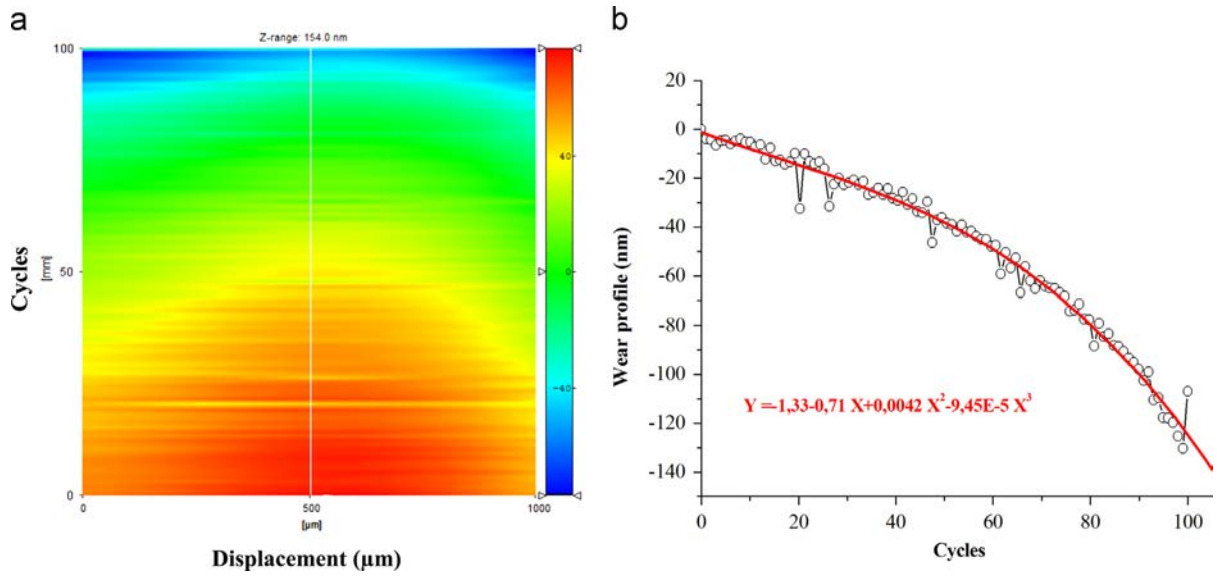


**Fig. 11.** (a) Typical wear map obtained during a nanotribological test carried out on a quartz resonator; (b) wear profile given the wear rate directly by fitting a polynomial curve on it. The initial offset is around 250 nm.

curved. In fact, this curvature is mainly due to the gold matter which is progressively pushed back to the extremities of the friction track during the test. After correction of the *initial offset* $z_0$ connected to the initial surface displacement, a polynomial fit on wear profiles gives a final depth around 138 nm. Taking into account the final area of the friction track ($5.44 \times 10^{-2}$ mm$^2$) and the gold density, the average wear weight lost per test is estimated at $144 \pm 12$ ng.

Results and their respective *wear rate* are all compiled in Table 1. Note that the *post mortem* wear rates are computed by assuming a linearly dependent wear process in contrast to the one computed with the *in situ* approach, which considers the change of slope at the 70th cycle. Considering the standard deviations of these results, *wear* and *wear rate* values obtained by these three approaches are very close to each other. Besides, the polynomial fit computed on *wear profiles* reveals that the wear assessed by the QCM approach corresponds to the one observed on the *wear map* at 95 cycles instead of 100 cycles, meaning a difference of 5%.

Our *in situ triboscopic* approach appears finally as a quite acceptable *quantitative* approach for the wear assessment at the nanoscale. This approach also enables the detection of any variation of the *wear rate* over time (as shown in Table 1). Thus, an average *wear rate* can be directly computed by using a profile analysis on the *wear map*. For instance, an average *wear rate* of 0.69 nm cycle$^{-1}$ has been obtained for the tribological test plotted in Fig. 8a corresponding to a tribocontact $Si_3N_4$/Silver carried out in the *zone* 1 at low friction regime (25 mN, 100 cycles, 1 mm/s, $z_0 = 35$ nm).

### 4.2. Applications to the soft and hard thin coatings nanowear assessment

#### 4.2.1. Nanowear of titanium and titanium oxide thin coatings deposited on glass substrates

Fig. 12 shows the evolution of the friction coefficient *vs.* normal load for titanium and titanium oxide thin coatings deposited on soda-lime glass substrate by sputtering physical vapor deposition [44,67,46,45]. Thicknesses of films are about 850 nm.

As expected, *soft* titanium film is submitted to a seizure phenomenon beyond a critical normal load (around 30 mN) in contrast to the *hard* titanium oxide film which displays a low and stable frictional behavior. The *in situ triboscopic* approach enables to understand the behavior beyond this threshold – *i.e.*, for a normal load of 40 mN. Note that the mechanical properties of each coatings have been identified with the procedure described in Section 2 and then reported in Table 2.

*Friction* and *wear maps* at 40 mN are plotted in Fig. 13a and b for the titanium and titanium oxide thin films, respectively. In both cases, wear depths are always lower than coatings thicknesses. However, *triboscopic* view enables us to accurately detect the seizure occurrence around 15 cycles for *soft* titanium film (Fig. 13a). On the

**Table 1**
Comparison of the wear assessments given by the three methods.

| Wear method | Wear amount (ng) | Wear rate (ng/cycle) |
|---|---|---|
| *Post mortem* QCM approach | 118 (15) | 1.18 |
| *Post mortem* profilometric approach | 106 (6) | 1.06 |
| *in situ* Triboscopic approach | 144 (12) | 0.89 for $0 < n_{cycles} \leq 70$<br>2.06 for<br>$70 < n_{cycles} \leq 100$ |

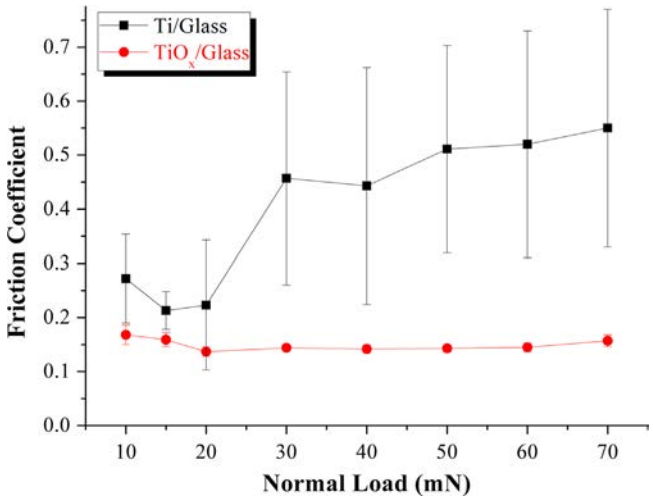


**Fig. 12.** Evolution of the friction coefficient vs. normal load for two kinds of PVD thin films coated on a glass substrate ($Si_3N_4$, v: 1 mm s$^{-1}$).

contrary, *friction* and *wear* behaviors are both homogeneous for the *hard* coating (Fig. 13b). Yet again, *triboscopic* assessment detects some differences between the two layers: height variations observed in Fig. 13a are mainly due to plastic deformation and ductility of titanium; no lasting tribolayer is then created. In contrast for the titanium oxide, Fig. 13b shows that a *cohesive tribolayer* is gradually built-up over time. Besides, this *tribolayer* clearly contributes to a low and stable frictional behavior. As a result wear rate of oxide is 2.5 times lower than that of the titanium.

#### 4.2.2. Nanowear of carbon nitrite coatings deposited on silicon wafer

Finally, Fig. 14a and b show the *friction* and *wear* maps obtained when a $Si_3N_4$ ball (Ø 1.5 mm) is rubbing on a 2.8 µm carbon nitride ($CN_6$) coating deposited on a polished mono-crystal (100) silicon wafer by using the PE-CVD technique [68,17]. This kind of coatings is frequently used in MEMS manufacturing [1,69,5,70,68,8]. The coating's mechanical properties were determined by the parametric identification of the stress–strain law: $E_f$: 325 GPa, $Y_f$: 8.75 GPa and $K_f$ : 0.253 GPa as described in Fig. 5c. The applied normal load and the sliding velocity are 70 mN and 1 mm $s^{-1}$, respectively. The correction of the initial offset is about 18 nm.

**Table 2**
Mechanical properties of the thin films coated on a glass substrate.

| Materials properties | Titanium thin film | Titanium oxide thin film |
|---|---|---|
| Young modulus $E$ (GPa) | 116 | 204 |
| Poisson's ratio $\nu$ | 0.32 | 0.25 |
| Yield stress $Y$ (MPa) | 191 | 866 |
| Initial correction $z_0$ (nm) | 38.7 | 24.1 |

From a *wear profile* extracted from the *wear map* (Fig. 14b), Fig. 15a reveals the presence of a time-dependent nanometric *tribolayer* (thickness: 40 nm) which is continuously built-up and destructed within the contact, as observed experimentally by Adachi et al. for carbon nitride coatings [69]. On a higher number of cycles (around 10,000 cycles), *wear rate* can be estimated from the wear profile at 0.18 nm/cycle.

As reported in a recent paper [19], the formation and destruction of this kind of *tribolayers* over time can also be studied by simulating the same tribocontact with a discrete approach called Movable Cellular Automata (MCA) [71], as illustrated in Fig. 15b. This numerical *wear profile* can be directly compared to the experimental one provided by the *in situ* triboscopic approach (Fig. 15a) in order to extract the parameters controlling the interactions between particles.

Indeed, since the *numerical* wear profile (Fig. 15b) is dependent on the interactions between particles, which are the simulation's parameters, the underlying mechanisms controlling the *cohesion* and *adhesion* of the *tribolayer* can be then studied by seeking the *optimal set* of interaction's parameters which provides a numerical

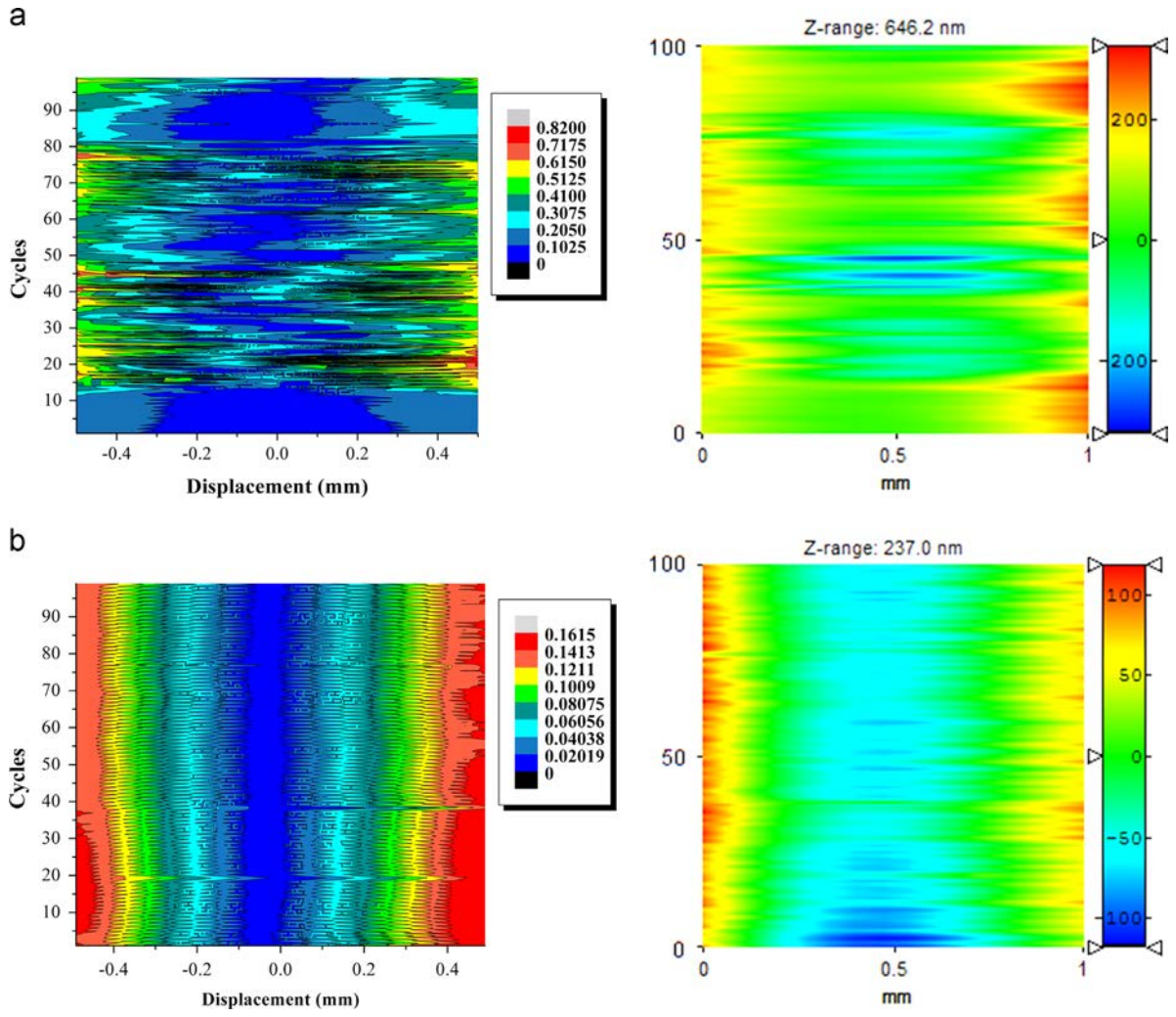


**Fig. 13.** *In situ* wear assessment of $Si_3N_4$/thin film coated on a glass substrate at 40 mN (100 cycles, 1 mm $s^{-1}$). (a) Triboscopic view obtained for titanium coated on a glass substrate: *friction map* (left) and *wear map* (right). (b) Triboscopic view obtained for titanium oxide coated on a glass substrate: *friction map* (left) and *wear map* (right).

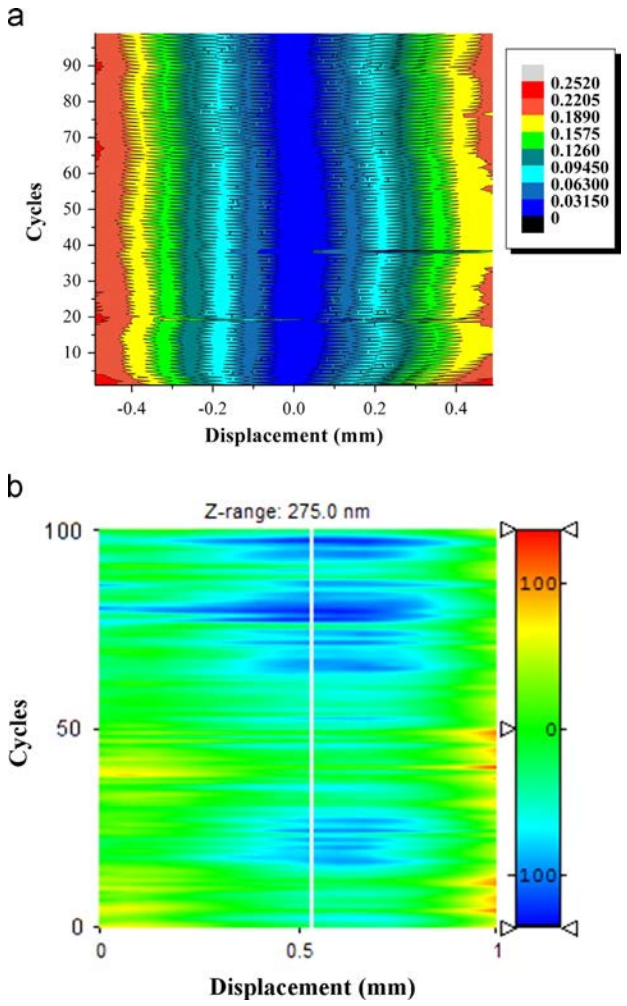


**Fig. 14.** Typical triboscopic view of $Si_3N_4/CN_6-Si(100)$ at 70 mN (100 cycles and 1 mm $s^{-1}$): (a) *friction map* and (b) *wear map*.

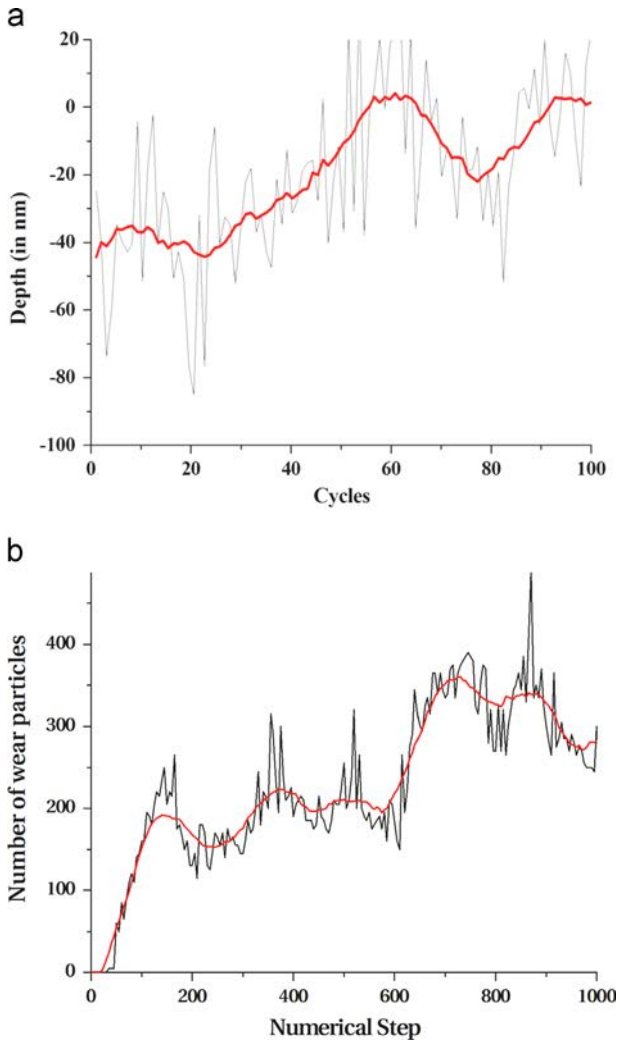


**Fig. 15.** Comparison between the wear profile obtained by (a) the *in situ* wear map (extracted from Fig. 14b) and (b) the numerical simulation of this tribocontact using the MCA approach [19].

*wear profile* that match correctly with the experimental one, for a same frictional behavior. Analyzing the final *optimal set*, some assumptions about the wear mechanisms that are likely to occur within the contact can finally be proposed. First results using this approach have been recently published [19].

## 5. Conclusion

Wear analysis at the micro/nanoscale is a great challenge for the MEMS/NEMS devices that are strongly affected by various surface phenomena such as friction/stiction, micro- and nanoscopic wear, surface contamination and environmental effects. At this scale classical *post mortem* analyses generally fail because (i) the elastic recovery is no longer negligible and (ii) the presence of a nanometric self-organized *tribolayer* within the contact, which often controls both friction and wear rate. To solve this problem and keep the *dynamic* relationship between friction and wear, an *in situ* wear assessment based method has been developed and presented in this paper. Its *key* process is based on a *triboscopic* approach where the real position of the ball during the test is known at any time in order to obtain the final position $z_f$ without opening the contact. This method depends, of course, on the mechanical properties of samples, which are determined by using an inverse method combining nanoindentation and boundary element numerical simulations. This approach was *qualitatively* and *quantitatively* validated and successfully applied on various thin coatings, which actually generate various kinds of *tribolayers*. In addition, results demonstrate that this *in situ* wear analysis is completely compatible with that computed by using discrete elements methods confirming then the possibility of coupling the two approaches in order to extract and identify the internal interactions occurring during the wear process.

## Acknowledgments

This work has been supported by the Labex ACTION project (contract “ANR-11-LABX-01-01”).

## References

[1] S. Achanta, J.-P. Celis, Nanotribology of MEMS/NEMS, Berlin, Heidelberg, 2007, pp. 522–547.
[2] B. Bhushan (Ed.), Nanotribology and Nanomechanics, an introduction, Springer-Verlag, Berlin-Heidelberg, 2005.
[3] B. Bhushan, Nanotribology and nanomechanics, Wear 259 (2005) 1507–1531.
[4] B. Bhushan, V. Koinkar, Micro-tribological studies of doped single-crystal silicon and polysilicon films for MEMS devices, Sens. Actuat. A 57 (1996) 91–102.
[5] T.-R. Hsu, MEMS & Microsystems, Design, Manufacture, & Nanoscale Engineering, 2nd ed., Wiley, 2008, Hoboken, New Jersey, 550p.
[6] S. Kim, D. Asay, M. Dugger, Nanotribology & MEMS, Nanotoday 2 (5) (2007) 22–29.

[7] N. Myshkin, A. Kovalev, W. Scharff, M. Ignatiev, The effect of adhesion on sliding friction at nanoscale, in: J. Bartz, F. Franek (Eds.), Proceedings of 3rd Vienna International Conference on Nanotechnology2009, pp. 323–328.
[8] S. Miyake, S. Yamazaki, Evaluation of protuberance and groove formation in extremely thin DLC films on Si substrates due to diamond tip sliding by atomic force microscopy, Wear 318 (2014) 135–144.
[9] M. Scherge, D. Shakhvorostov, K. Pöhlmann, Fundamental wear mechanism of metals, Wear 255 (2003) 395–400.
[10] R. Colaço, An AFM study of single-contact abrasive wear: the Rabinowicz wear equation revisited, Wear 267 (2009) 1772–1776.
[11] E. Meyer, R. Lüthi, Tribological experiments with friction force microscopy, in: H. Nalwa (Ed.), Handbook of Nanostructured Materials and Nanotechnology, vol. 2, 2000, pp. 345–383.
[12] L. Peng, H. Lee, W. Teizer, H. Liang, Nanowear of gold and silver against silicon, Wear 267 (2009) 1177–1180.
[13] M. Brendlé, P. Diss, P. Stempflé, Nanoparticle detachment: a possible link between macro- and nanotribology? Tribol. Lett. 9 (2000) 97–104.
[14] M. Brendlé, P. Stempflé, Triboreactions of graphite with moisture—a new model of triboreactor for integrating friction and wear, Wear 254 (2003) 818–826.
[15] P. Stempflé, J. von Stebut, Nano-mechanical behaviour of the 3rd body generated in dry friction—feedback effect of the 3rd body and influence of the surrounding environment on the tribology of graphite, Wear 260 (2006) 601–614.
[16] P. Stempflé, F. Pollet, L. Carpentier, Influence of intergranular metallic nanoparticles on the fretting wear mechanisms of Fe–Cr–Al2O3 nanocomposites rubbing on Ti–6Al–4V, Tribol. Int. 41 (2008) 1009–1019.
[17] P. Stempflé, J. Takadoum, Multi-asperity nanotribological behaviour of single-crystal silicon: crystallography-induced anisotropy in friction and wear, Tribol. Int. 48 (2012) 35–43.
[18] P. Stempflé, O. Pantalé, T. Djilali, R. Kouitat Njiwa, X. Bourrat, J. Takadoum, Evaluation of the real contact area in three-body dry friction by micro-thermal analysis, Tribol. Int. 43 (2010) 1794–1805.
[19] P. Stempflé, A. Domatti, H. Dang, J. Takadoum, Mechanical and chemical wear components in environmental multi-asperity nanotribology, Tribol. Int. 82 (2015) 358–374 ⟨http://dx.doi.org/10.1016/j.triboint.2014.04.036i⟩.
[20] S. Achanta, D. Drees, J.-P. Celis, Investigation of friction on hard homogeneous coatings during reciprocating tests at micro-Newton normal forces, Wear 263 (2007) 1390–1396.
[21] C. Mate, Tribology on the Small Scale, Oxford University Press, NY, 2008.
[22] R. Nevshupa, M. Scherge, S.I.-U. Ahmed, Transitional microfriction behaviour of silicon induced by spontaneous water adsorption, Surf. Sci. 517 (2002) 17–28.
[23] N. Ohmae, J.-M. Martin, S. Mori, Micro- and Nanotribology, ASME Press, NY, 2005.
[24] M. Scherge, Scale dependence of friction, in: Proceedings of the World Tribology Congress, 2001, pp. 31–37.
[25] J. Yu, L. Qian, B. Yu, Z. Zhou, Nanofretting behaviors of monocrystalline silicon (100) against diamond tips in atmosphere and vacuum, Wear 267 (2009) 322–329.
[26] G. Fox-Rabinovich, G. Totten (Eds.), Self-Organization During Friction: Advanced Surface-Engineered Materials and Systems Design, CRC Press, Boca Raton, 2006.
[27] M. Nosonovsky, Self-organisation at the frictional interface for green tribology, Philos. Trans. R. Soc. A 368 (2010) 4755–4774.
[28] E. Meyer, R. Overney, K. Dransfeld, T. Gyalog, Nanoscience—Friction & Rheology on the Nanometer Scale, World Scientific, London, 2008.
[29] J.-E. Schmutz, H. Fuchs, H. Hölscher, Measuring wear by combining friction force and dynamic force microscopy, Wear 268 (2010) 526–532.
[30] R. Colbert, B. Krick, A. Dunn, J. Vail, N. Argibay, W. Sawyer, Uncertainty in pin-on-disk wear volume measurements using surface scanning techniques, Tribol. Lett. 42 (2011) 129–131.
[31] D. Shakhvorostov, L. Jian, E. Nold, G. Beuchle, M. Scherge, Influence of Cu grain size on running-in related phenomena, Tribol. Lett. 28 (2007) 307–318.
[32] D. Burris, W. Sawyer, Addressing practical challenges of low friction coefficient measurements, Tribol. Lett. 35 (2009) 17–23.
[33] I. Szlufarska, M. Chandross, R. Carpick, Recent advances in single-asperity nanotribology, J. Phys. D: Appl. Phys. 41 (2008) 123001.
[34] N. Tambe, Nanotribology: Nanotribological Investigations of Materials, Coatings and Lubricants at High Sliding Velocities for Nanotechnology Applications, Verlag Dr. Müller, 2009.
[35] R. Ahmed, A. Ashraf, M. Elameen, N. Faisal, A. El-Sherik, Y. Elakwah, M. Goosen, Single asperity nanoscratch behaviour of HIPed and cast Stellite 6 alloys, Wear 312 (2014) 70–82.
[36] B. Bhushan, Contact mechanics of rough surfaces in tribology: multiple asperity contact, Tribol. Lett. 4 (1998) 1–35.
[37] H. Liu, I.-U. Ahmed, M. Scherge, Microtribological properties of silicon and silicon coated with DLC, OTS and STCd salt films: a comparative study, Thin Solid Films 381 (2001) 135–142.
[38] E.-S. Yoon, R. Singh, H.-J. Oh, H. Kong, The effect of contact area on nano/micro-scale friction, Wear 259 (2005) 1424–1431.
[39] H. Heshmat, Tribology of Interface Layers, CRC Press, Boca Raton, 2010.
[40] M. Belin, J.-M. Martin, Triboscopy, a new approach to surface degradations of thin films, Wear 156 (1992) 151–160.
[41] M. Scherge, K. Pöhlmann, A. Gervé, Wear measurement using radionuclide-technique (RNT), Wear 254 (2003) 801–817.
[42] T. Feser, P. Stoyanov, F. Mohr, M. Dienwiebel, The running-in mechanisms of binary brass studied by in situ topography measurements, Wear 303 (2013) 465–472.
[43] S. Korres, M. Dienwiebel, Design and construction of a novel tribometer with on-line topography and wear measurement, Rev. Sci. Instrum. 81 (2010) 063904.
[44] A. Lakhtaria, R. Messier, Sculptured thin Films, Nanoengineered Morphology and Optics, SPIE Press Bellingham, Washington USA, 2005.
[45] P. Stempflé, A. Besnard, N. Martin, A. Domatti, J. Takadoum, Accurate control of friction with nanosculptured thin coatings: application to gripping in microscale assembly, Tribol. Int. 59 (2013) 67–78. http://dx.doi.org/10.1016/j.triboint.2012.05.026.
[46] H. Yaghoubi, N. Taghavinia, E. Keshavarz Alamdari, A. Volinsky, Nanomechanical properties of TiO2 granular thin films, Appl. Mater. Interf. 2 (9) (2010) 2629–2636.
[47] X. Chen, Computational modeling of indentation, in: M. Oyen (Ed.), Handbook of Nanoindentation, Pan Stanford Publishing, Cambridge, 2011, pp. 153–183.
[48] A. Faraji, Elastic and Elastoplastic Contact Analysis: Using Boundary Elements & Mathematical Programming, WIT Press, Southampton, UK, 2005.
[49] N. Oumarou, R. Kouitat Njiwa, J.-P. Jehl, P. Stempflé, On the variation of mechanical parameters obtained from spherical depth sensing indentation, Int. J. Surf. Sci. Eng. 4 (4/5/6) (2010) 416–428.
[50] I. Polonsky, L. Keer, Elastic–plastic microcontact modeling using dislocations, in: D. D., et al., (Eds.), The Third Body Concept, Elsevier Science, Amsterdam, The Nederlands, 1996, pp. 55–66.
[51] R. Kouitat Njiwa, J. von Stebut, Three dimensional boundary element analysis of internal cracks under sliding contact load with a spherical indenter, Eng. Fract. Mech. 71 (2004) 2607–2620.
[52] R. Kouitat Njiwa, R. Consiglio, J. von Stebut, Boundary element modelling of coated materials in static and sliding ball-flat elastic contact, Surf. Coat. Technol. 102 (1998) 148–153.
[53] B. Persson, Slid. Frict.: Phys. Princ. Appl. (2000) 528.
[54] I.-H. Sung, H.-S. Lee, D. Kim, Effect of surface topography on the frictional behaviour at the micro/nano-scale, Wear 254 (2003) 1019–1031.
[55] P. Stempflé, et al., Thermal-induced wear mechanisms of sheet nacre in dry friction, Tribol. Lett. 35 (2009) 97–104.
[56] P. Wriggers, Computational Contact Mechanics, John Wiley & Sons Ltd., Chichester, UK, 2002.
[57] A. Fischer-Cripps, Nanoindentation, Springer-Verlag, NY, 2002.
[58] J. Alcala, et al., The influence of plastic hardening on surface deformation modes around Vickers and spherical indents, Acta Mater. 48 (2000) 3451–3464.
[59] P. Stempflé, F. Schäfer, Hybrid algorithm for identifying the nanomechanical properties of materials and thin films, Int. J. Surf. Sci. Eng. 1 (2/3) (2007) 213–238.
[60] J. Dreo, A. Pétrowski, P. Siarry, E. Taillard, Metaheuristics for Hard Optimization: Methods and Case Studies, Springer-Verlag, Berlin, Heidelberg, 2006.
[61] F. Glover, M. Laguna, Tabu Search, Kluwer Academic Publishers, Norwell, USA, 1998.
[62] S. Campbell, et al., Modeling and Simulation in Scilab/Scicos, 2nd ed., Springer-Verlag, NY, 2009.
[63] N. Oumarou, R. Kouitat Njiwa, P. Stempflé, J. von Stebut, On the deformation of a hard coating/soft substrate system under spherical nanoindentation: a boundary element numerical analysis, J. Tribol. Surf. Eng. 1 (1–2) (2010) 111–128.
[64] G. Beer, Programming the Boundary Element Method, Wiley, Chichester, UK, 2001.
[65] A. Markus, Modern FORTRAN in Practice, Cambridge University Press, Cambridge, New York, Melbourne, Madrid, Cape Town, Singapore, Sao Paulo, Delhi, Mexico City, 2012.
[66] G. Liu, G. Zhang, QCM-D Studies on Polymer Behavior at Interfaces, Springer, Heidelberg, New York, Dordrecht, London, 2013.
[67] Y. Gaillard, V. Rico, E. Jimenez-Pique, A. Gonzalez-Elipe, Nanoindentation of TiO2 thin films with different microstructures, J. Phys. D: Appl. Phys. 42 (2009) 145305.
[68] J. Takadoum, J.-Y. Rauch, J.-M. Cattenot, N. Martin, Comparative study of mechanical and tribological properties of CNx and DLC films, Surf. Coat. Technol. 174–175 (2003) 427–433.
[69] K. Adachi, K. Kato, Tribology of carbon nitride coatings, in: C. Donnet, A. Erdemir (Eds.), Tribology of Diamond-like Carbon Films, Springer, New York, USA, 2008, pp. 339–361.
[70] A. Khurshudov, K. Kato, D. Sawada, Tribological and mechanical properties of carbon nitride thin coating prepared by ion-beam-assisted deposition, Tribol. Lett. 2 (1) (1996) 13–21.
[71] S. Psakhie, Y. Horie, G. Ostermeyer, S. Korostelev, A. Smolin, E. Shilko, A. Dmitriev, S. Blatnik, M. Spegel, S. Zavsek, Movable cellular automata method for simulating materials with mesostructure, Theor. Appl. Fract. Mech. 37 (2001) 311–334.